

Modulation of superconductivity by a magnetic template in Nb/BaFe₁₂O₁₉ hybrids

Zhaorong Yang,* Koen Vervaeke, and Victor V. Moshchalkov†

INPAC, Institute for Nanoscale Physics and Chemistry, K. U. Leuven, Celestijnenlaan 200D, B-3001 Leuven, Belgium

Ritta Szymczak

Polish Academy of Sciences, Institute of Physics, al. Lotnikow 32/46, Warszawa 02-668, Poland

(Received 27 December 2005; revised manuscript received 9 April 2006; published 12 June 2006)

Inhomogeneous magnetic fields generated by the BaFe₁₂O₁₉ ferromagnetic substrate create a *magnetic template* for superconducting condensate in the Nb/BaFe₁₂O₁₉ hybrids. Depending on the field and temperature, the magnetic template guides superconductivity to nucleate in different areas: above the magnetic domain walls of the BaFe₁₂O₁₉ forming the domain-wall superconductivity (DWS), above the reversed magnetic domains (RDS), and above the positive magnetic domains forming bulk superconductivity. The DWS, behaving as a superconducting wire network, survives in a broad field range. The RDS, existing in the form of isolated superconducting islands near the saturation field H_s of BaFe₁₂O₁₉, can be described as a two-dimensional two-component random conductor mixture. Being related to the hysteretic domain evolution, superconducting condensate above the reversed domains shows pronounced switching behavior.

DOI: 10.1103/PhysRevB.73.224509

PACS number(s): 74.25.Dw, 74.78.Db, 75.47.-m

Intensive research efforts have been devoted recently to the enhancement of the superconducting critical parameters (critical temperature T_c , field H_{c2} , and current I_c) aimed at a broader spectrum of applications of superconductors.¹ One way to control the critical parameters is to confine the superconducting condensate through nanostructuring.² When the size of the superconducting material becomes of the same order as the coherence length ξ or the magnetic penetration depth λ , the electrical and magnetic properties of the used materials are strongly influenced by the boundary conditions. In this case the nanostructured materials can exhibit different superconducting properties. Another way to tailor the critical parameters can be achieved by introducing a magnetic template created by a ferromagnetic subsystem.^{3–11} Although superconductivity and magnetism are often thought to be a antagonistic phenomena, recent studies on superconductor-ferromagnet (*S/F*) hybrids revealed that the interaction between superconducting and magnetic order parameters at the micro- and nanometer length scale can lead to a number of new physical phenomena like the spin switch superconductivity,¹⁰ or magnetic-field-induced superconductivity.¹¹

Recently, we presented the experimental observation of the domain-wall superconductivity (DWS) in Nb/BaFe₁₂O₁₉ hybrids.¹² With the decrease of temperature in zero applied magnetic field, we found that the superconductivity in the Nb film first appears just above the domain walls of BaFe₁₂O₁₉. In this paper, we focus on the nucleation of superconductivity in the areas above reversed domains (RDS) of the BaFe₁₂O₁₉, and systemically study the evolution of DWS and RDS with temperature and field. We found that the DWS, behaving as a superconducting wire network, survives in a broad field range. The RDS, induced by reversed domains (RD), exists in the form of isolated superconducting islands near the saturation field H_s of BaFe₁₂O₁₉. The critical temperature $T_c(H)$ of the RDS is enhanced compared to that of a reference Nb sample. By switching between different magnetic states, the superconducting critical parameters can be effectively controlled.

The Nb/BaFe₁₂O₁₉ sample has been prepared by depositing 50 nm Nb film on the single crystal BaFe₁₂O₁₉ (0001) substrate ($420 \times 420 \times 90 \mu\text{m}^3$) by molecular beam epitaxy. A 10 nm Si layer was used as a buffer between Nb and BaFe₁₂O₁₉. Hexagonal BaFe₁₂O₁₉ is a well-known ferrimagnet with a uniaxial anisotropy along its [0001] direction. The magnetization loop measured at 5 K with the field applied perpendicular to (0001) shows that the saturation field H_s of the BaFe₁₂O₁₉ is about 6 kOe, the nucleation field H_n is about 4.75 kOe, and the saturation magnetization is about 491 G s.¹² The domain structure of the BaFe₁₂O₁₉(0001) substrate has been investigated by magnetic force microscopy (MFM) at room temperature by ramping the field from remanent state towards saturation and back again along the major hysteresis loop. The evolution of the domain structure is shown in Fig. 1. At low fields [panel (b)], the MFM image displays a branched domain pattern with the domain wall width of about 200 nm. With increasing field, the branched domains transform into isolated bubble domains at fields near H_s [panel (e)]. Above H_s [panel (c)], the contrast is almost homogeneous. When the field is ramped down from the saturation, reversed domains [panel (d)] start to nucleate at H_n . The evolution of the domain structure displays clear hysteresis due to the difference between H_s and H_n . No evident hysteresis is observed at low fields, i.e., the domain walls move freely in response to the variation of the external field.

The magnetic stray field above the BaFe₁₂O₁₉ substrate surface has been recorded directly by scanning Hall probe microscopy (SHPM) at room temperature and in zero applied magnetic field. The size of the Hall sensor is $0.8 \mu\text{m}$. The image [Fig. 2(a)] covers an area of $35 \mu\text{m} \times 40 \mu\text{m}$. The gray scale of the image runs from -60 Gauss (black areas, where magnetic field goes into the sample) to $+74$ Gauss (white areas, where magnetic field comes out of the sample). Branched stripe domains, with a width varying roughly between $5 \mu\text{m}$ and $10 \mu\text{m}$, are visible. In the middle of the stripe domains, localized domains with reversed magnetiza-

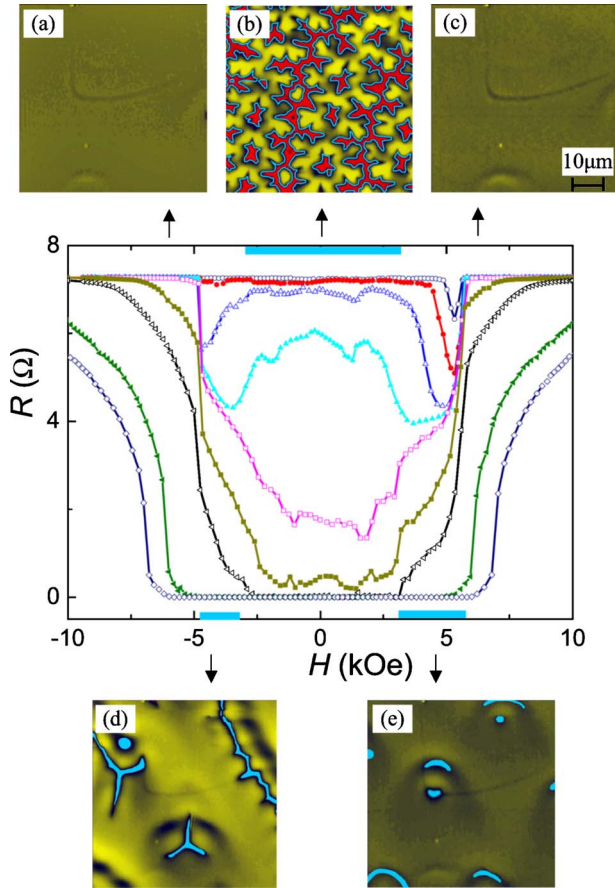


FIG. 1. (Color online) Field dependence of resistance R for Nb/BaFe₁₂O₁₉ at different temperatures: 8.1 K, 8.0 K, 7.9 K, 7.8 K, 7.6 K, 7.3 K, 7.1 K, 6.7 K, 6.5 K (from top to bottom). With increasing field from -10 kOe to 10 kOe, the domain pattern of BaFe₁₂O₁₉ evolves as follows: saturation (a); nucleation of reversed domains (d); branched domains (b); isolated reversed domains before saturation (e); saturation (c).

tion (darker spots in white domains and brighter spots in dark domains) exist due to the domain branching. Taking a cross section of the image [Fig. 2(a)] allows us to quantify the magnetic field variations [Fig. 2(b)]. Across different domains, the stray field changes smoothly. In the SHPM technique the magnetic field is measured at about $1 \mu\text{m}$ above the sample. Closer to the surface much higher magnetic fields and better resolution can thus be expected.

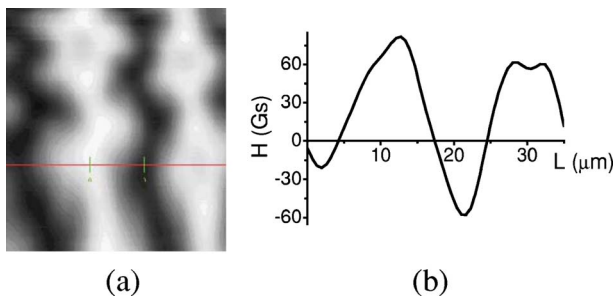


FIG. 2. (Color online) (a) SHPM image of a BaFe₁₂O₁₉ surface at room temperature. (b) Cross section of the SHPM image along the line shown in Fig. 2(a).

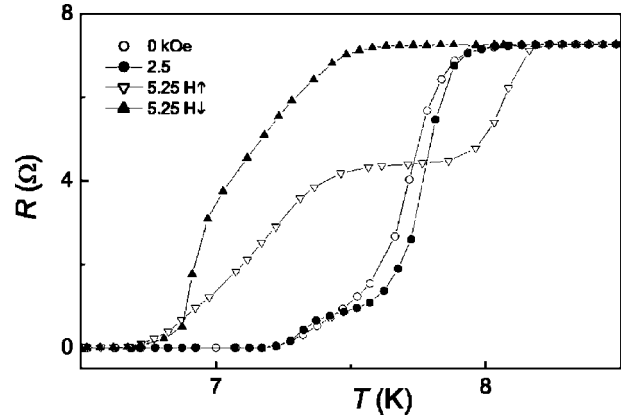


FIG. 3. Temperature dependence of resistance R for Nb/BaFe₁₂O₁₉ at different H . H is ramped as follows: 0 kOe (open circles) \rightarrow 2.5 kOe (filled circles) \rightarrow 5.25 kOe (open triangles) \rightarrow saturation \rightarrow 5.25 kOe (filled triangles).

The resistance R of the Nb film deposited on BaFe₁₂O₁₉ was measured in a Physical Properties Measurement System (Quantum Design) applying a four-probe ac technique with an ac current of $10 \mu\text{A}$ at a frequency of 19 Hz. The main panel of Fig. 1 shows the resistance as a function of field at various fixed temperatures. The magnetic field H is applied perpendicular to the sample surface in the sequence from -10 kOe to 10 kOe. At $T_0=8.1$ K, the resistance $R(H, T_0)$ displays a single dip only near the saturation field $+H_s$ of BaFe₁₂O₁₉, and no traces of superconductivity are present at $-H_s$. As the temperature is decreased, the dip broadens, the resistance at low fields decreases, and another dip develops in the negative field region corresponding to the nucleation of reversed domain in BaFe₁₂O₁₉ at $-H_n$. Clearly, the onset of superconductivity is magnetic field polarity dependent. The dips and the decrease of resistance in low fields can be attributed to the existence of RDS and DWS, respectively. Between 7.8 K and 7.6 K, the resistance at low fields decreases drastically with temperature. As a result, the dips in resistance disappear below 7.6 K.

To understand the evolution of DWS and RDS, we shall first have a closer look at the domain structure of BaFe₁₂O₁₉ (Fig. 1). For DWS, because of the nature of filamentary conduction, superconducting current flows along the branched domain walls and forms a superconducting wire network¹³ [see blue (white) lines in panel (b)]. In contrast to that, RDS appears above the reversed domains and forms isolated superconducting islands [see blue (white) areas in panels (d) and (e)]. The DWS forms more easily percolative conducting path and reaches the zero resistance state, in comparison to RDS. As the temperature is decreased, the resistance at low fields drops abruptly (Fig. 1). Consequently, the S/F structure shows a relatively sharp resistive superconducting transition at zero field and two-steps superconducting transition at 5.25 kOe (Fig. 3).

With increasing field from zero, the domain walls move freely, and so do the superconducting paths. Therefore, the conducting paths between the voltage contacts change with field because of the shift of the domain walls. Due to the rearrangement of the conducting paths in response to the

variation of magnetic field, the measured resistance fluctuates. The superconducting areas can be compared to a random superconducting network below the percolation threshold.^{14,15} As seen from Fig. 1, no dip is observed at zero field and the resistance changes in a broad field range. As the field is swept from -2.5 kOe to 3.1 kOe, the system enters the zero field state almost at the same temperature of 7.1 K. The superconducting network seems to be only weakly influenced by the applied magnetic field of this magnitude. From Fig. 3 we can see that the resistance measured at 2.5 kOe has almost the same behavior as the zero field resistance, i.e., the DWS survives in a broad field range.

It is interesting to note that in the DWS theory of Aladyshkin *et al.*, the width of the domain wall has been considered to be zero.¹⁶ With this assumption, the applied magnetic field is believed to suppress the localized superconducting nucleus and the DWS exists only at a relatively weak applied field. For the $\text{BaFe}_{12}\text{O}_{19}$ single crystal, however, the domain wall width is about 200 nm, which is much larger than the superconducting coherence length in our Nb films, $\xi(0) \approx 6.67$ nm.¹² Across the domain wall, the stray field decreases gradually from $+H_d$ to $-H_d$, here H_d is the stray field above the magnetic domains [Fig. 2(b)]. In this case, with the decrease of temperature, superconductivity in zero applied field $H_a=0$ must first appear just above the middle of the domain wall because in that area the stray fields are the lowest. An application of an external magnetic field results in a partial or complete compensation of the stray field above the domain wall, and favors the superconductivity to nucleate in the place corresponding to the minimum of the total magnetic field. As a result, the superconducting area will shift away from the middle to the boundary of the domain wall, provided that the latter has a polarity opposite to that of the applied field.

Keeping in mind that the applied field compensates not only in the stray field above the domain wall, but also in the stray field above the reversed domain, by further increasing the field to a certain magnitude, the area with the lowest total magnetic field $|H_a - H_d|$ will shift from the domain wall to the reversed domain. Consequently, the superconductivity can no longer be confined by the domain walls and will start to occupy the areas above the reversed domains. In Nb/ $\text{BaFe}_{12}\text{O}_{19}$, the stray field H_d above the reversed domains is about 5.4 kOe.¹² At 5.25 kOe, because of the field compensation effect between H_a and H_d , the onset of the superconducting transition temperature T_c (8.2 K) is higher than that measured at zero field (Fig. 3). In contrast to that, a reference sample (50 nm Nb deposited on Si/SiO₂ substrate with 10 nm Si as buffer layer between Nb and Si/SiO₂) has a much lower onset temperature of superconducting transition at 5.25 kOe (7.4 K). Clearly, due to the field compensation by the reversed domains, the superconducting critical temperature $T_c(H)$ is enhanced at large applied fields.

The presence of the isolated RDS islands [Fig. 1(e)] is revealed by the shape of the $R(T)$ curve at 5.25 kOe (Fig. 3), which displays two steps in the superconducting transition. This is in contrast to the $R(T)$ curve measured when the same field 5.25 kOe is attained from saturation [the typical MFM pattern is like panel (a) in Fig. 1]. In that case, the onset

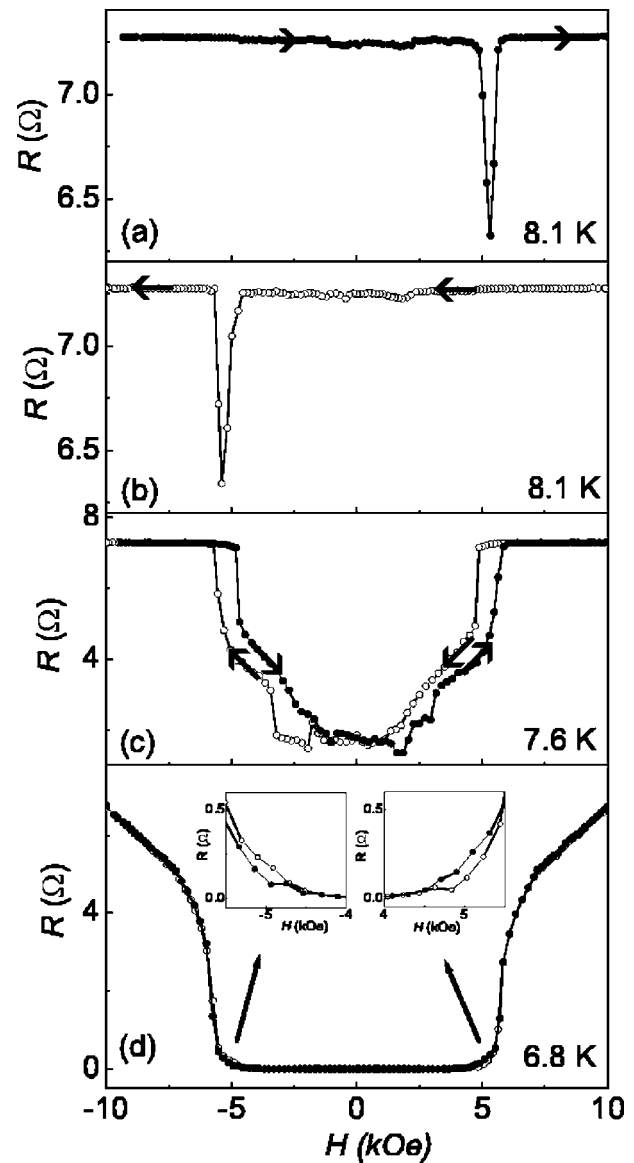


FIG. 4. Evolution of hysteretic resistive transitions with temperature in Nb/ $\text{BaFe}_{12}\text{O}_{19}$. The field is first swept from -10 kOe to $+10$ kOe (filled circles) and then back from $+10$ kOe to -10 kOe (open circles). The insets in (d) are enlarged views of $R(H)$ curves around the saturation field of $\text{BaFe}_{12}\text{O}_{19}$.

temperature of the superconducting transition is almost equal to the onset temperature of the second step. In both magnetic states zero resistance is reached almost at the same temperature. Therefore, the second step in the resistive transition in the reversed domain state can be attributed to the appearance of superconductivity above positive magnetic domains, which forms bulk superconductivity.

For pure RDS, the measured global resistance depends not only on the field compensation effect but also on the total area of available reversed domains.¹² Being related to the hysteretic domain evolution, the resistive $R(H)$ transition depends on the magnetic field history (Fig. 4). At 8.1 K, the resistance shows a sharp dip at fields near $+H_s$ as the field is swept from -10 kOe to 10 kOe. The dip can be seen at a negative field $-H_s$ if the field is swept from 10 kOe

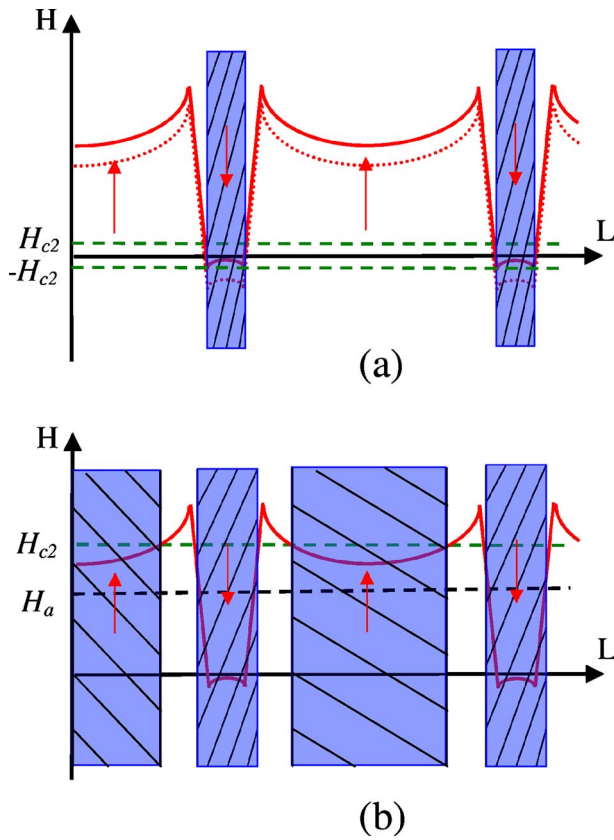


FIG. 5. (Color online) Schematic illustrations of the magnetic field distribution in the superconducting layer in the reversed domain state. Dashed lines indicate the upper critical field H_{c2} and the applied field H_a . Red (dark gray) lines show the total magnetic field $H_a + H_d$. (a) For high temperatures with small H_{c2} ; (b) for low temperatures with large H_{c2} .

to -10 kOe. When the field is ramped down from 10 kOe (or -10 kOe), the dip near $+H_s$ (or $-H_s$) is erased, suggesting the suppression of the RDS. As we further increase the field again from zero, the dip recovers again exactly in the same field region. Depending on the field history, the superconductivity can be switched either on or off. With decreasing temperature, the dip broadens. At 7.6 K, although no dips can be found due to the evolution of DWS in low field region, the RDS is almost completely suppressed above H_n . Below H_n , the resistance decreases abruptly, signaling the onset of superconductivity above the reversed domains. With further decreasing temperature, accompanying the appearance of bulk superconductivity near H_s , the hysteresis becomes less pronounced. Before the disappearance of the hysteresis, an opposite hysteretic behavior is observed at 6.8 K in comparison to $T=7.6$ K [see Fig. 4(d)].

Figure 5 schematically illustrates the typical magnetic field distribution in the superconducting film at fields near H_s .¹⁷ For the magnetic state with reversed domains, the maximum total magnetic field is located around them. Far away from the boundary of the reversed domains, the total field decays and displays a minimum at the center of the positive domains. To induce the superconductivity above the reversed domains, the applied field should comply with the constraint $|H_a - H_d| < H_{c2}$, which limits the field range for

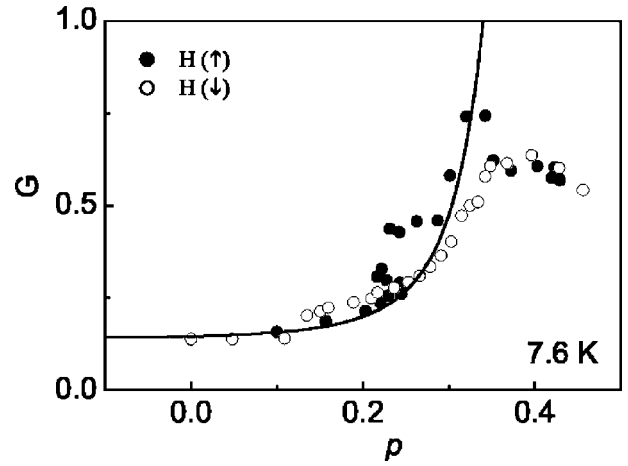


FIG. 6. Conductance G as a function of the reversed domain area p at 7.6 K. p was derived from the MFM data in Ref. 12 by dividing the red area (reversed domain) by the total area. Solid line is fit according to the scaling formula $G - G_0 = a(p_c - p)^{-s}$.

the RDS appearance. At $T \approx 8.1$ K, the H_{c2} is so small that the constraint is fulfilled only in a narrow field region around H_d [see the red (dark gray) solid line in Fig. 5(a)], leading to the sharp magnetoresistance dip in Fig. 4(a). As the field is deviated from H_d by $\pm H_{c2}$, the RDS is suppressed, see the red (dark gray) dotted line in Fig. 5(a). This is the reason why no traces of superconductivity are present at negative fields in Fig. 4(a). With decreasing temperature, the H_{c2} increases, the field range for the appearance of RDS expands, therefore the dip broadens. At $T \approx 6.8$ K, because of the large value of H_{c2} , the superconductivity not only exists above reversed domains, but also in the areas above the center of the positive domains forming the bulk superconductivity [see blue (dark gray) areas in Fig. 5(b)]. In this case, the superconductivity is mainly suppressed around the reversed domains due to the maximum total field there. The system can therefore be viewed as consisting of RDS, bulk superconductivity, and normal state metal. Because of the isolated nature of RDS, the onset of the zero resistance state is determined by the percolation through superconducting areas. In contrast to that, the field distribution is more homogeneous when the field is ramped down from saturation to H_n . As a result of the homogenous field distribution, the measured resistance is lower as displayed in Fig. 4(d). Below H_n , both have a comparable domain structure [panels (d) and (e) of Fig. 1], and no evident hysteresis is observed.

At low fields, superconductivity survives only above the domain walls which form a superconducting wire network. At $T \geq 7.6$ K, superconductivity spreads from the domain wall to the reversed domain areas as the field is ramped up towards H_s . At lower temperatures, the superconducting areas spread not only to reversed domains, but also to the center of the positive domains. For both cases, the superconducting wire network transforms into a binary composite consisting of superconducting islands and normal metal. Figure 6 shows conductance as a function of the area of the reversed domains at 7.6 K. The RD area p was derived by image processing of the MFM data presented in Ref. 12. At temperatures above 7.6 K, we found that the conductance

increases with the area of the reversed domains at low p value. For higher p value or lower temperatures, the conductance is dominated by DWS or bulk superconductivity, and the correlation between conductance and the RD area is not applicable. For two-dimensional two-component random-conductor mixture, below the percolation threshold p_c (~ 0.5), the conductance is believed to exhibit a power-law behavior,¹⁸ $G \sim (p_c - p)^{-s}$. Using this scaling formula, with the critical exponent $s=4.23$ and $p_c=0.5$, the experimentally observed conductance can be reasonably well described (see Fig. 6).

In conclusion, the effects of magnetic template on the superconducting state in Nb/BaFe₁₂O₁₉ hybrids have been studied. At low fields, the DWS, confined in domain wall

area, forms a superconducting wire network. At fields near H_s , the superconductivity, induced by the reversed domains, has higher onset critical temperature of the superconducting transition compared to a reference Nb sample. By switching between different magnetic states, the superconducting critical parameters can be effectively controlled.

We would like to thank M. Lange for help with the measurements and useful discussions, and A. Volodin for MFM measurements. This work is supported by the K. U. Leuven Research Fund No. GOA/2004/02, Flemish FWO, Belgian IUAP and Bilateral Flanders-China Project No. BIL 04/03 Programmes.

*Present address: Key Laboratory of Materials Physics, Institute of Solid State Physics, Chinese Academy of Sciences, Hefei 230031, People's Republic of China. Electronic address: zryang@issp.ac.cn

†Author to whom correspondence should be addressed. Electronic address: Victor.Moshchalkov@fys.kuleuven.be

¹V. V. Moshchalkov, V. Bruyndoncx, L. Van Look, M. J. Van Bael, Y. Bruynseraede, and A. Tonomura, *Handbook of Nanostructured Materials and Nanotechnology* (Academic, San Diego, 2000), Vol. 3, Chap. 9, p. 451.

²V. V. Moshchalkov, L. Gielen, C. Strunk, R. Jonckheere, X. Qiu, C. Van Haesendonck, and Y. Bruynseraede, *Nature* (London) **373**, 319 (1995).

³For recent reviews, see I. F. Lyuksyutov and V. L. Pokrovsky, *Adv. Phys.* **54**, 67 (2005); A. I. Buzdin, *Rev. Mod. Phys.* **77**, 935 (2005).

⁴I. F. Lyuksyutov and V. L. Pokrovsky, *Phys. Rev. Lett.* **81**, 2344 (1998).

⁵S. Erdin, I. F. Lyuksyutov, V. L. Pokrovsky, and V. M. Vinokur, *Phys. Rev. Lett.* **88**, 017001 (2002).

⁶J. I. Martin, M. Velez, J. Nogues, and I. K. Schuller, *Phys. Rev.*

Lett. **79**, 1929 (1997).

⁷L. N. Bulaevskii, E. M. Chudnovsky, and M. P. Maley, *Appl. Phys. Lett.* **76**, 2594 (2000).

⁸D. S. Golubović, W. V. Pogosov, M. Morelle, and V. V. Moshchalkov, *Appl. Phys. Lett.* **83**, 1593 (2003).

⁹A. Yu. Rusanov, M. Hesselberth, J. Aarts, and A. I. Buzdin, *Phys. Rev. Lett.* **93**, 057002 (2004).

¹⁰J. Y. Gu *et al.*, *Phys. Rev. Lett.* **89**, 267001 (2002).

¹¹M. Lange, M. J. Van Bael, Y. Bruynseraede, and V. V. Moshchalkov, *Phys. Rev. Lett.* **90**, 197006 (2003).

¹²Z. R. Yang, M. Lange, A. Volodin, R. Szymczak, and V. V. Moshchalkov, *Nat. Mater.* **3**, 793 (2004).

¹³J. Maps, D. D. Berkley, J. H. Kang, and A. M. Goldman, *Phys. Rev. B* **35**, 38 (1987).

¹⁴X. S. Ling *et al.*, *Phys. Rev. Lett.* **76**, 2989 (1996).

¹⁵D. C. Wright, D. J. Bergman, and Y. Kantor, *Phys. Rev. B* **33**, 396 (1986).

¹⁶A. Y. Aladyshkin *et al.*, *Phys. Rev. B* **68**, 184508 (2003).

¹⁷Hans J. Hug *et al.*, *J. Appl. Phys.* **79**, 5609 (1996).

¹⁸D. C. Hong, H. E. Stanley, A. Coniglio, and A. Bunde, *Phys. Rev. B* **33**, 4564 (1986).